NASA's Infrared Telescope Facility (IRTF) on 3 June 1996 by J. R. Spencer, personal communication.
20. D. C. Pieri *et al.*, *Icarus* **60**, 685 (1984).
21. D. L. Blaney *et al.*, *ibid.* **113**, 220 (1995); J. R. Spencer and N. M. Schneider, *Annu. Rev. Earth Planet. Sci.* **24**, 125 (1996).
22. A. S. McEwen and L. A. Soderblom, *Icarus* **55**, 191 (1983).
23. R. B. Minton, *Comm. Lunar Planet. Lab* **10**, 35 (1973).
24. R. M. Nelson and B. W. Hapke, *Icarus* **36**, 304 (1978).
25. T. V. Johnson *et al.*, *Geophys. Res. Lett.* **22**, 3293 (1995).
26. A. S. McEwen *et al.*, *J. Geophys. Res.* **90**, 12345 (1985).
27. J. C. Pearl and W. M. Sinton, in *Satellites of Jupiter*, D. Morrison, Ed. (Univ. of Arizona Press, Tucson, 1982), p. 724; D. Morrison and C. Telesco, *Icarus* **44**, 226 (1980).
28. A. F. Cook *et al.*, *Science* **211**, 1419 (1981); the Voyager wide-angle camera was sensitive to emissions between 380 and 600 nm. The SSI camera is sensitive to emissions in a much wider band, 380 to 1050 nm.
29. F. Scherb and W. H. Smyth, *J. Geophys. Res.* **98**, 18729 (1993).
30. E. Lellouch *et al.*, *Icarus* **98**, 271 (1992); G. Ballester *et al.*, *ibid.* **111**, 2 (1994); E. Lellouch, *ibid.*, in press; P. Sartoretti *et al.*, *ibid.*, in press.
31. B. K. Lucchitta and L. A. Soderblom, in *Satellites of Jupiter*, D. Morrison, Ed. (Univ. of Arizona Press, Tucson, 1982), p. 521; M. C. Malin and D. C. Pieri in *Satellites*, J. A. Burns and M. S. Matthews, Eds. (Univ. of Arizona Press, Tucson, 1990), p. 689. With a diameter of 3138 km and a mean density of 3040 kg/m^3, Europa is comparable in many respects to Earth's moon but contains at least 5% by mass of water (*32*). Earth-based spectroscopy shows the surface to be predominantly water ice (*33*). Although the water could be contained mostly in hydrated minerals (*34*), most models of the interior involve an outer shell of water as thick as 100 km, parts of which could be liquid (*35*). Local darkening of the surface could result from ice weathering and contamination by rocky materials (*36*). The general paucity of impact craters observed in the Voyager data suggested a youthful surface and the possibility of recent, or even active, resurfacing.
32. G. Schubert *et al.*, in *Satellites*, J. A. Burns and M. S. Matthews, Eds. (Univ. of Arizona Press, Tucson, 1990), p. 224.
33. C. B. Pilcher *et al.*, *Science* **178**, 1087 (1972).
34. A. A. Finnerty *et al.*, *Nature* **289**, 24 (1981).
35. P. Cassen *et al.*, *Geophys. Res. Lett.* **6**, 731(1979); G. W. Ojakangas and D. J. Stevenson, *Icarus* **81**, 220 (1989).
36. A. S. McEwen, *J. Geophys. Res.* **91**, 8077 (1990).
37. M. P. Golombek and E. Bruckenthal, *Lunar Planet. Sci.* **XIV**, 251 (1983).
38. G. D. Crawford and D. J. Stevenson, *Icarus* **73**, 66 (1988).
39. P. M. Schenk and W. B. McKinnon, *ibid.* **79**, 75 (1989).
40. P. H. Schenk, *J. Geophys. Res.* **98**, 7475 (1993).
41. A. S. McEwen, *Icarus* **81**, 220 (1990).
42. T. V. Johnson *et al.*, *J. Geophys. Res.* **88**, 5789 (1983); A. S. McEwen, *ibid.* **91**, 8077 (1986); D. Domingue and B. Hapke, *Icarus* **99**, 70 (1992).
43. B. Lucchitta, *Icarus* **44**, 481 (1980); E. Shoemaker *et al.*, in *The Satellites of Jupiter*, D. Morrison, Ed. (Univ. of Arizona Press, Tucson, 1982), p. 435.
44. Post-Voyager discussion of graben, modified tension fractures, and ductile necking features can be found in the following: J. Fink and R. Fletcher, *NASA Tech. Memo. TM-84211* (1981), p. 51; E. Shoemaker *et al.*, in *The Satellites of Jupiter*, D. Morrison, Ed. (Univ. of Arizona Press, Tucson, 1982), p. 435; E. M. Parmentier *et al.*, *Nature* **395**, 290 (1982); and S. W. Squyres, *Icarus* **52**, 545 (1982). Mass wasting and differences in strain rate or thickness of the lithosphere are discussed by Parmentier *et al.* and Squyres. Constructional ice-volcanism or surface deformation due to ice plutonism in underlying fractures is discussed by S. Croft *et al.*, *Icarus* **73**, 279 (1988).
45. See, for example, the discussion by S. W. Squyres and S. K. Croft in *Satellites*, J. A. Burns and M. S. Matthews, Eds. (Univ. of Arizona Press, Tucson, 1990), p. 293.
46. M. P. Golombek and M. Allison, *Geophys. Res. Lett.* **8**, 1139 (1981); S. J. Murchie *et al.*, *J. Geophys. Res.* **91**, E222 (1990); E. M. Parmentier *et al.*, *Nature* **295**, 290 (1982).
47. J. E. Guest *et al.*, *U.S. Geol. Surv. Misc. Invest. Ser. Map I-1934* (1988).
48. S. J. Murchie *et al.*, *J. Geophys. Res.* **91**, E222 (1990); R. Cassachia and R. Strom, *ibid.* **89**, B419 (1984); P. Shenk and W. McKinnon, *Icarus* **72**, 209 (1987); M. Zube and E. Parmentier, *ibid.* **60**, 200 (1984); E. M. Shumaker *et al.*, in *Satellites of Jupiter*, D. Morrison, Ed. (Univ. of Arizona Press, Tucson, 1932), p. 435.
49. E. M. Shoemaker *et al.*, in *Satellites of Jupiter*, D. Morrison, Ed. (Univ. of Arizona Press, Tucson, 1982), p. 435.
50. S. J. Murchie *et al.*, *J. Geophys. Res.*, **91**, E222 (1990).
51. B. Lucchitta *et al.*, *U.S. Geol. Surv. Misc. Inv. Ser. Map* I-2289 (1992).
52. P. Helfenstein, thesis, Brown University, Providence, RI (1990); *Lunar Planet. Sci.* **XVII**, 333 (1990); P. Schenk and W. McKinnon, *Icarus* **89**, 318 (1989); S. J. Murchie *et al.*, *Lunar Planet. Sci.* **XXIII**, 943 (1992).
53. We thank the current project manager, W. J. O'Neil, and his predecessors J. R. Casani and R. J. Spehalski for their leadership; T. Brady and J. Marr for flight software development and its implementation; G. Levanas and his team for their diagnosis of the tape recorder problems and the creation of a safe way to operate this device; and W. Cunningham and his team who provided the new SSI camera flight software. T. Becker, E. Lee, R. Sucharski, and T. Rosanova provided the team with maps. Many associates of team members contributed to the success of the SSI experiment; we thank N. Ausman, E. A. Alvarez del Castillo, K. Bender, H. Breneman, K. Buxbaum, T. Colvin, D. Deats, T. Denk, S. Fagents, A. DiCicco, P. Helfenstein, S. Henderson, K. Homan, T. Jones, J. M. Kaufman, R. Kirk, J. Klemaszewski, S. LaVoie, E. Lo, L. Lowes, K. Magee, W. Merline, R. Mitchell, H. Mortensen, B. Paczkowski, C. Phillips, K. Rages, A. Simon, D. Simonelli, J. N. Spitale, C. Stanley, E. Ustinov, D. Winther, D. Johnson, J. Van der Woude, J. Yatteau, A. Culver, D. Jensen, D. Alexander, and J. Yoshimizu. We acknowledge the contributions of absent colleagues H. Masursky, J. Pollack, C. Yeates, and J. Dunne. A portion of this research was carried out by the Jet Propulsion Laboratory, California Institute of Technology, under contract with NASA. The National Optical Astronomy Observatories are operated by the Association of Universities for Research in Astronomy (AURA), under cooperative agreement with the National Science Foundation.

24 September 1996; accepted 1 October 1996

Near-Infrared Spectroscopy and Spectral Mapping of Jupiter and the Galilean Satellites: Results from Galileo's Initial Orbit

R. Carlson,* W. Smythe, K. Baines, E. Barbinis, K. Becker, R. Burns, S. Calcutt, W. Calvin, R. Clark, G. Danielson, A. Davies, P. Drossart, T. Encrenaz, F. Fanale,† J. Granahan,† G. Hansen, P. Herrera, C. Hibbitts, J. Hui, P. Irwin, T. Johnson, L. Kamp, H. Kieffer, F. Leader, E. Lellouch, R. Lopes-Gautier, D. Matson, T. McCord,† R. Mehlman, A. Ocampo, G. Orton, M. Roos-Serote, M. Segura, J. Shirley, L. Soderblom, A. Stevenson, F. Taylor, J. Torson, A. Weir, P. Weissman

The Near Infrared Mapping Spectrometer performed spectral studies of Jupiter and the Galilean satellites during the June 1996 perijove pass of the Galileo spacecraft. Spectra for a 5-micrometer hot spot on Jupiter are consistent with the absence of a significant water cloud above 8 bars and with a depletion of water compared to that predicted for solar composition, corroborating results from the Galileo probe. Great Red Spot (GRS) spectral images show that parts of this feature extend upward to 240 millibars, although considerable altitude-dependent structure is found within it. A ring of dense clouds surrounds the GRS and is lower than it by 3 to 7 kilometers. Spectra of Callisto and Ganymede reveal a feature at 4.25 micrometers, attributed to the presence of hydrated minerals or possibly carbon dioxide on their surfaces. Spectra of Europa's high latitudes imply that fine-grained water frost overlies larger grains. Several active volcanic regions were found on Io, with temperatures of 420 to 620 kelvin and projected areas of 5 to 70 square kilometers.

In late June 1996, the Galileo spacecraft obtained its first remote sensing measurements within the jovian system. The Near Infrared Mapping Spectrometer (NIMS) performed spectroscopic and spectral mapping measurements of Jupiter's atmosphere and the surfaces of the Galilean satellites. The NIMS instrument (*1*) has a modest spectral resolving power of 40 to 200 from 0.7 to 5.2 μm, but combines this with spatial coverage at a resolution of 300 to 800 km for Jupiter and a few to several hundred kilometers for the Galilean satellites. A large number of atmospheric molecules, surface minerals, and condensates exhibit diagnostic spectral signatures in the NIMS range, so the measurements represent a powerful tool for investigating a wide range of processes on Jupiter and its moons. Here we present some results from the first orbital pass, which provided coverage of the planet and all four Galilean satellites (*2*).

Initial observations concentrated on two prominent and mysterious features of Jupiter's atmosphere: 5-μm hot spots and the GRS. Hot spots are regions where the upper cloud cover is relatively thin, so that thermal emission from the warm lower atmosphere escapes and can be observed by NIMS, especially at wavelengths in the spectral window near 5 μm where the gaseous absorption is also low. The Galileo entry probe descended into such a region (*3*), and made compositional and other measurements. Two striking findings were the low abundance of water vapor relative to solar composition models of Jupiter and the absence of the predicted dense water cloud (*4*). NIMS measurements in hot spots probe down to pressures of several bars, so interesting comparisons are possible, and NIMS can extend the probe data to the global scale.

Spectra were obtained for a targeted hot spot, identified prior to Galileo's orbital pass using ground-based telescopes. The location of these spectra are shown superimposed on a contemporaneous ground-based image (Fig. 1) and span the feature from center to edge. Thermal emission is strongest at the center (Fig. 2), where the reflected solar intensity at 1.1 and 2.7 μm is lowest (Fig. 3), as would be expected if the hot spot was indeed produced by a localized thinning of the main cloud deck. Within ammonia bands the opposite was found—the intensity of reflected light was greater in the hot spot, even though the clouds were presumably thinner there—suggesting that ammonia was depleted within the hot spot. The lower ammonia content may be connected with the low water vapor amounts, that is, hot spots may be generally dry with respect to all condensates relative to their surroundings, or may be a result of reduced amounts of ammonia ice as part of the general reduction in cloud cover (*5*). Curiously, however, a high thin cloud, thought to be ammonia cirrus, appeared to be enhanced over the hot regions surrounding the GRS (compare Fig. 4, C and D).

Thermal emission spectra in the 4- to 5.5-μm region show features attributed to minor constituents that are present in the jovian troposphere, specifically germane (GeH_4), phosphine (PH_3), and deuterated methane (CH_3D), as well as water vapor, ammonia, and methane. The observed spectrum of Fig. 2 can be fit with computed synthetic spectra (*6*) based on the measurements by the Galileo entry probe (*7*). Although our synthetic spectra do not give a unique fit to the data, we find that the NIMS spectra are consistent with the absence of a water cloud in the range sounded (5 to 8 bars), and that water mixing ratios are well below that which would be expected if Jupiter were well mixed and had a solar abundance of oxygen. We also find that there is a fairly thick cloud (optical depth of approximately 1 at 5 μm) at a high level, again consistent with the probe, which placed this cloud at about 1.5 bars.

The GRS was observed at several phase and hour angle combinations and in spectral bands with different absorption strengths, enabling vertical sounding of the clouds and providing information about particles within it (Fig. 4). It can be seen that the GRS system had a high-altitude core (Fig. 4C), evident in the 1.76-μm methane absorption band which cloaks the lower atmosphere and is useful for sounding high clouds. This core was offset to the east, upwind relative to the prevailing jet flow, and showed considerable structure, which was different in each channel. The core was surrounded by a

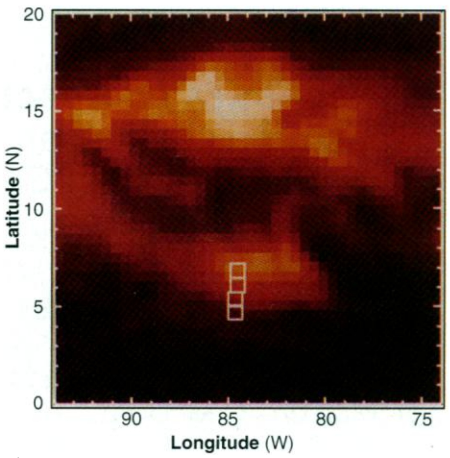

Fig. 1. 4.8-μm image of the hot spot, obtained 28 June 1996 at the NASA IRTF at Mauna Kea, Hawaii, using NSFCAM. The location of the four NIMS pixels are shown, each being 850 km in width and height. The northernmost pixel occurs at 7.0°N. This hot spot disappeared 2 days later. Possible latitude and longitude errors for the pixel assemblage are about one half to one pixel.

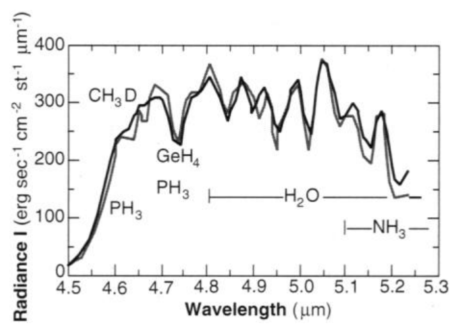

Fig. 2. Hot spot thermal emission spectrum (in gray), for the end pixel of Fig. 1 located within the hot spot. Absorption regions are indicated for various molecules. A model fit is shown in black and based partly upon the Probe measurements; see (*6*, *7*).

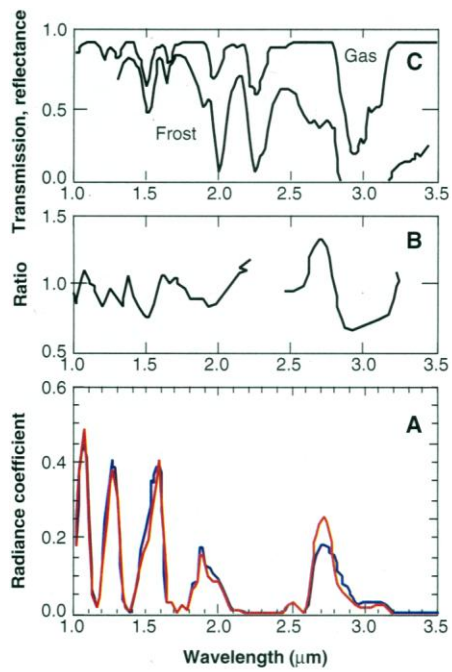

Fig. 3. Spectra in the reflected sunlight region. (**A**) NIMS spectra inside the hot spot (red) and outside (blue), the end pixels in Fig. 1. A Lambertian surface would have a radiance coefficient of unity. (**B**) Ratio of the spectra outside the hot spot to inside it. (**C**) Transmission spectrum of NH_3 gas and a reflection spectrum of NH_3 frost (*4*). Note that the minima in the ratio spectrum (B) correlate with ammonia gas and frost absorption features (C).

R. Carlson, W. Smythe, K. Baines, R. Burns, A. Davies, P. Herrera, J. Hui, T. Johnson, L. Kamp, R. Lopes-Gautier, D. Matson, A. Ocampo, G. Orton, M. Segura, J. Shirley, A. Stevenson, P. Weissman, Jet Propulsion Laboratory, California Institute of Technology, Pasadena, CA 91109, USA.
E. Barbinis, F. Leader, R. Mehlman, Institute of Geophysics and Planetary Physics, University of California, Los Angeles, CA 90095, USA.
S. Calcutt, P. Irwin, F. Taylor, A. Weir, Department of Atmospheric, Oceanic, and Planetary Physics, Oxford University, Oxford OX1 3PU, UK.
K. Becker, W. Calvin, H. Kieffer, L. Soderblom, J. Torson, U.S. Geological Survey, Flagstaff, AZ 86001, USA.
R. Clark, U.S. Geological Survey, Denver, CO 80225, USA.
G. Danielson, Division of Geological and Planetary Science, California Institute of Technology, Pasadena, CA 91125, USA.
P. Drossart, T. Encrenaz, E. Lellouch, M. Roos-Serote, Observatoire de Paris, Meudon 92150, France.
F. Fanale, J. Granahan, G. Hansen, C. Hibbitts, T. McCord, Hawaii Institute of Geophysics and Planetology, University of Hawaii, Honolulu, HI 96822, USA.

*To whom correspondence should be addressed.
†Also at SETS Technology, Inc., Mililani, HI 96789, USA.

bright ring, evident in both the 0.76- and 2.7-μm images but absent in the 1.76-μm image, indicating that it was lower in altitude. This ring in turn was surrounded by a region of relatively clear atmosphere, like an extended hot spot (Fig. 4D), which passed either side of the GRS but was much wider to the north. As noted above, there was a high altitude haze associated with this relatively clear region, which can be seen clearly in Fig. 4C. Thermal emission features were abundant, occurring even within the GRS.

NIMS multiwavelength imagery within various absorption bands of well-mixed gases (primarily H_2 and CH_4) can be used for quantitative evaluation of the cloud top pressure levels, among other parameters. Using a two-cloud model, with the top of the upper cloud determined from the measured radiances and radiative-transfer calculations (8), we find that the highest regions of the GRS extended to a pressure level of 240 mbar, approximately 20 km above its assumed base at 700 mbar. The eastern portion of the surrounding ring, at its brightest point (Fig. 4, A and B), is lower than the GRS peak by approximately 3 km (pressure of ~280 mbar). The western portion of the ring is even lower, by about 4 km (pressure of ~340 mbar), from the brightest eastern point.

We obtained spectra of Callisto at low spatial resolution (650 km) and high phase angle (123°). These spectra (for example, Fig. 5) show some weak water ice features, but the spectra are dominated by structure indicative of the presence of hydrated minerals (including possible hydroxides), as the OH stretching transition near 3 μm is strong but the shorter wavelength water bands are nearly absent (9). A new absorption feature was observed in Callisto's spectrum at 4.25 μm (Fig. 5), and its strength appears to vary with position on Callisto. One possible source for this absorption is CO_2 (perhaps as a clathrate) in small concentrations (~0.5% by weight). Preferred candidates include hydrated and hydroxylated minerals exhibiting combination transitions such as OH(stretch)-M-OH(bending) (M represents a metal atom such as Mg, Al, or Fe). A number of materials exhibit such transitions near 4.3 μm; future analysis and additional spectra from later orbits will allow a more definitive identification.

Ganymede was targeted for close flyby during the first orbit of Galileo and was mapped globally at modest spatial resolution (~100 km). Three spectra from representative areas (Marius Regio, Uruk Sulcus, and the bright-rayed crater Osiris) are shown in Fig. 6. The bright regions of Osiris exhibit strong water ice bands, whereas the water bands are modified and shifted in Marius Regio and Uruk Sulcus, indicating the presence of hydrated minerals in these regions (9). A 4.25-μm feature was also

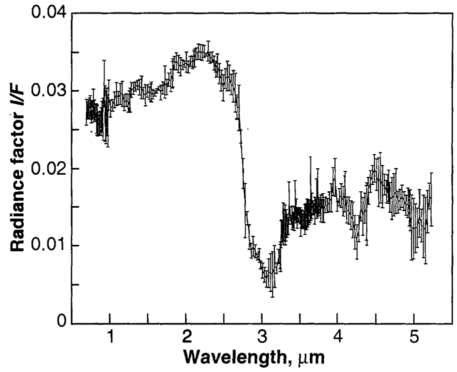

Fig. 5. Callisto spectrum. This *I/F* spectrum (*I* is radiance and πF is the solar irradiance) is an average of four pixels which show the least amount of water ice features. The previously unreported absorption at 4.25 μm could arise from hydrated or hydroxylated minerals or CO_2 perhaps in clathrate form.

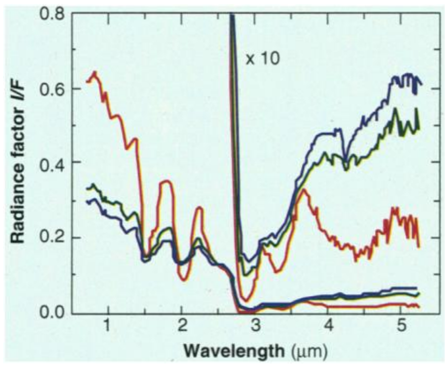

Fig. 6. Ganymede *I/F* spectra. Three regions are represented: the bright Osiris rays (red), Uruk Sulcus (green), and Marius Regio (blue). At long wavelengths, the same spectra are shown with a factor of 10 enhancement. Note the 4.25-μm feature in the Marius Regio spectrum. The noise level is ~ 0.005 in *I/F* at long wavelengths.

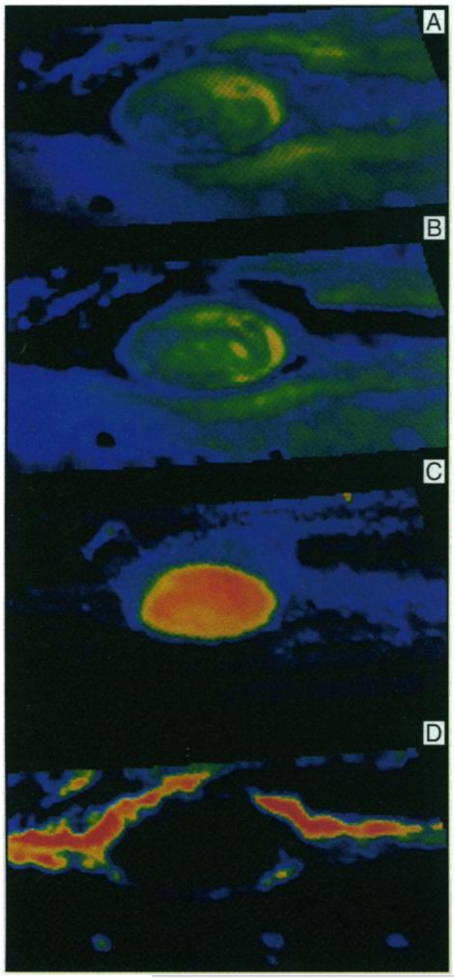

Fig. 4. Spectral images of the GRS. (**A**) is for a continuum wavelength of 0.76 μm and shows the visual appearance of the clouds, largely unaffected by absorption, (**B**) 2.73-μm image, which probes slightly higher and is sensitive to ammonia ice absorption. Differences between (A) and (B) can arise from spatially variable cloud particle properties. (**C**) Image (1.76 μm) which senses clouds at relatively high altitudes. (**D**) Thermal emission at 4.99 μm, showing net cloud transparency. In all cases, red represents the highest intensity.

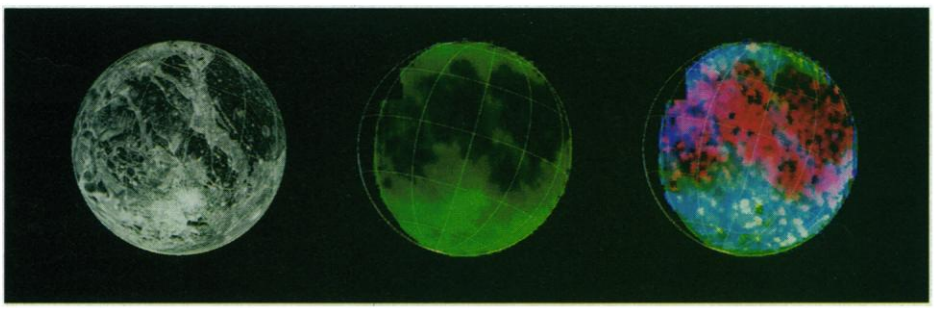

Fig. 7. Band depth maps of Ganymede and a comparison Voyager map. (**Left**) is a digital mosaic of Ganymede. (**Middle**) shows the 2-μm band depth variation. (**Right**) is a false-color composite of the 1.5- and 2-μm band depths (blue and green color planes, respectively) and the depth of the 4.25-μm feature (red).

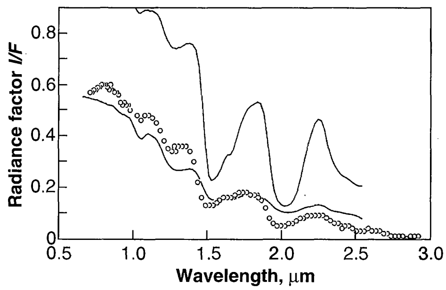

Fig. 8. Spectrum of Europa in the northern polar region, shown as the open circles and representing a region at approximately 60°N, 270°W. Two laboratory measurements (*11*) of water ice are shown; the upper curve is for a thick layer of 200-μm grains whereas the lower curve is for a thin layer of fine-grained frost on an ice surface. The fine-grained surface frost reduces the apparent strength of the 1.5- and 2-μm bands, but is sufficiently transparent that photons penetrate into the lower ice to produce the relatively strong 1.04- and 1.25-μm absorptions. Note the similarity of Europa's spectrum with the lower curve. The noise level of Europa's spectrum is smaller than the plotting symbol.

found on Ganymede but is generally weaker than that found on Callisto.

A 2.0-μm band-depth map (Fig. 7, middle) illustrates that water ice is nonuniformly distributed over the surface; water ice is relatively depleted in the visually dark regions (Fig. 7, left). Other factors such as temperature, purity, grain size, and the presence of hydrated species can influence the band depth, so this abundance map is only approximate. A false-color image (Fig. 7, right), which incorporates band depths at 1.5 μm (in blue) and 2.0 μm (in green), shows that the surface ice grain properties are fairly uniform in the icy areas. The depth of the 4.25-μm feature is mapped in red, illustrating that the mineral causing this absorption is distributed at low latitudes, implying more exposure of non–water ice material. The 1.04-μm water ice absorption is also stronger in the equatorial region, implying that ice grains are larger there. These two observations, along with the apparent fine-grained frosts in the polar regions, may suggest that water migrates from the equator to the poles. However, O_2 also absorbs at 1.05 μm and may complicate this interpretation.

Among the jovian moons, Europa has long been thought to have the largest amount of pure water ice on its surface on the basis of full-disk telescopic studies (*10*). NIMS obtained spectral maps with coverage of the northern polar regions (Fig. 8). The spectral shape resembles telescopic spectra for the trailing hemisphere (*10*) and is consistent with a fine-grained water frost overlaying a coarser grained ice component or a glazed surface [see Fig. 8 and (*11*)].

Several discrete regions of volcanic activity were found on Io, each showing blackbody-like emission between 2 and 5 μm. The hemisphere observed was that with central meridian longitude of 135°W. An area of $\sim$15 km^2 near the equator at approximately 90°W longitude was found to be emitting at a temperature of 460 K. This region may correspond to the active site Hi'iaka found in 1990 ground-based observations (*12*). The Amirani region was found to emit at 510 K with a projected area of 40 km^2 while emission from the vicinity of Prometheus showed temperature of 590 K and a projected area of 7 km^2. Other hot areas range from 420 K to 620 K, with corresponding areas of 70 and 5 km^2.

REFERENCES AND NOTES

1. R. Carlson, P. R. Weissman, W.D. Smythe, J. C. Mahoney, *Space Sci. Rev.* **60**, 457 (1990).
2. During the first orbit, the instrument suffered a transient memory anomaly, which rendered some part of the data not useful. It is thought that particle radiation effects altered the instrument memory, eventually halting the processor. Some Io monitoring observations as well as GRS spectra and spectral images were lost. The instrument has been successfully reset and is ready for upcoming orbits.
3. The Galileo Probe entered at 6.5°N [R. Young, M. A. Smith, C. K. Sobeck. *Science* **272**, 837 (1996)], just within a hot spot (G. Orton *et al.*, *ibid.*, p. 839).
4. Probe results are given by H. Niemann *et al.*, *ibid.*, p. 846 and B. Ragent *et al.*, *ibid.*, p. 854. Theoretical predictions of three cloud layers including a lower H_2O cloud were made by S. J. Weidenschilling and J. S. Lewis, *Icarus* **20**, 465 (1973).
5. The ammonia ice reflectance spectrum of Fig. 2 is from U. Fink and G. Sill, in *Comets*, L. Wilkening, Ed. (Univ. of Arizona Press, Tucson, 1982), pp. 164–202. The ammonia gas spectrum was computed for a vertical path starting at the 1 bar level and an ammonia mixing ratio of 14 ppmv, using absorption coefficients from I. Kleiner, G. Tarrago, Q-L. Kou, G. Guelachvili, L. Brown, 14th International Conference on High Resolution Molecular Spectroscopy, Prague, September 1996. Both spectra are evaluated for the NIMS spectral resolution.
6. We used two independent line-by-line radiative transfer models [after P. Drossart and T. Encrenaz, *Icarus* **52**, 483 (1982); also E. Lellouch, P. Drossart, T. Encrenaz, *ibid.* **77**, 457 (1989); and P. Irwin *et al.*, *Adv. Space Sci.*, in press].
7. A dry adiabatic temperature profile was employed [A. Seiff *et al.*, *Science* **272**, 844 (1996); A. Seiff, personal communication] with the following abundances: H_2O, 1% of saturation for a pressure of <4 bars and 20% solar O abundance for pressures between 8.5 and 11 bars (H. Niemann *et al.*, *ibid.*, p. 846; S. Atreya, personal communication); NH_3, strong depletion above 3 bars ($q = [NH_3]/[H_2] = 3.5$ ppmv at 0.5 bar) and 1.5 times solar abundance below (L. Sromovsky *et al.*, *ibid.*, p. 851; S. Atreya, personal communication, 1996); PH_3 and GeH_4 from Voyager IRIS spectra [V. Kunde *et al.*, *Astrophys. J.* **263**, 443 (1982)]; and CH_3D, 0.25 ppmv. The opacity of the pressure-induced translation-rotation transition of H_2 was from J. Borysow, L. Trafton, L. Frommhold, and G. Birnbaum [*Astrophys. J.* **296**, 644 (1985)]. A single cloud with a base at 1.5 bars [B. Ragent, D. S. Colburn, P. Avrin, K. A. Rages, *Science* **272**, 854 (1996)] was modeled as a gray absorbing layer.
8. We used the radiative transfer method of K. H. Baines and W. H. Smith, *Icarus* **85**, 65 (1990). Methane absorption values were augmented with low-temperature infrared correlated-k opacities from K. H. Baines, R. A. West, L. P. Giver, and F. Moreno [*J. Geophys. Res.* **98**, 5517 (1993)] and visible absorption coefficients from E. Karkoschka and M. G. Tomasko [*Icarus* **97**, 161 (1992)]. The simple two-cloud layer which was used incorporated a partially absorbing reflector (single scattering albedo $w = 0.99$) overlain by a putative NH_3 cloud of variable physical and optical thicknesses (to be determined from the data). This cloud was characterized by the aerosol parameters of M. G. Tomasko, R. A. West, and N. D. Castillo [*Icarus* **33**, 558 (1978)], a particle-to-gas scale height ratio of unity, and a cloudbase at 0.7 bars (that is, the NH_3 condensation level).
9. R. Clark, T. V. V. King, M. Klejwa, G. A. Swayze, N. Vergo, *J. Geophys. Res.* **95**, 12653 (1990).
10. For a review of the icy Galilean satellite spectra see W. M. Calvin, R. N. Clark, R. H. Brown, J. R. Spencer, *ibid.* **100**, 19041 (1995).
11. R. Clark, *ibid.* **86**, 3087 (1981).
12. J. R. Spencer, *Annu. Rev. Earth Planet. Sci.* **24**, 125 (1996).

13. We thank the Galileo staff who reprogrammed the spacecraft, tested the combined system, and successfully brought back the acquired data. For CDS programming efforts: T. Brady, D. Erickson, F. Ford, E. Greenberg, B. Jaffe, B. Miller, E. Nicolich, and D. Winther; for devising the NIMS lossless data compression algorithm, R. Rice; for testing support: G. Laborde, C. Compton, M. Orozco, M. Molander, Q. Chau, J. Mirelez, W. Currie, J. Dodds, R. Nava, G. Levanas, R. Morgan, T. Verbich, H. Tran, A. Tallman, R. Scrivner, R. Wendlandt, M. Fahid, W. Hoffman, A. Vaughs, B. Bennett, B. Beaudry, E. Imlay, T. Neilson, P. Donatucci, G. LaBorde, K. McGraw, E. Nilsen, G. Snyder, J. Glance, P. Broer, M. Varuna, J. Michael, and D. Bluhm; for inflight loads: R. Barry, N. Simon, R. Weaver, and other members mentioned earlier; for playback support: A. Dicicco and J. Culwell; for observation design: B. Cracchiola and L. Crowell; for ground data support: H. Mortenson, D. Jenson, D. Knight, S. Noland, C. Stanley, and J. Yoshimizu; and for computer and general support: T. Arakelian, N. Cline, J. Alonzo, and J. Gardner. Portions of the work described herein was performed at the Jet Propulsion Laboratory, California Institute of Technology, under contract with the National Aeronautics and Space Administration.

9 September 1996; accepted 30 September 1996